Timosaponin AIII Disrupts Morphological Plasticity and Migration of Breast Adenocarcinoma Through Inhibition of Integrin Internalisation

Takeshi Terabayashi
Oita University: Oita Daigaku https://orcid.org/0000-0001-7102-784X
Katsuhiro Hanada
Oita University: Oita Daigaku
Shigeru Matsuoka
Oita University: Oita Daigaku
Takako Sasaki
Oita University: Oita Daigaku
Akira Katoh
Oita University: Oita Daigaku
Takahiro Akamine
Oita University: Oita Daigaku
Toshimasa Ishizaki (t-ishizaki@oita-u.ac.jp)
Oita University: Oita Daigaku

Research Article

Keywords: Tiomosaponin AIII, morphological plasticity, migration, lamellipodia, integrin internalisation

Posted Date: March 15th, 2021

DOI: https://doi.org/10.21203/rs.3.rs-276535/v1

Abstract

Cell migration is a critical step in tumour invasion and metastasis. To acquire invasive properties, cancer cells use their surrounding environment through dynamic and bidirectional interactions and change their morphology and mode of migration. Thus, inhibition of morphological plasticity regulated by paracrine interactions may be a promising approach for anti-cancer therapy. In this study, we found that timosaponin AIII (TAIII), a steroidal saponin isolated from the roots of *Anemarrhena asphodeloides*, disrupted the morphological changes and migratory activity of breast adenocarcinoma cells promoted by paracrine interactions with mammary epithelium-derived cells. TAIII suppressed lamellipodia formation of MDA-MB-231 cells in response to exogenous stimuli from MCF10A cells, thereby inhibiting morphological changes and migration. TAIII also attenuated membrane spreading and induced contraction of HeLa cells, followed by expansion of intercellular gaps. Furthermore, we analysed the intracellular dynamics of TAIII labelled with a fluorescent dye and found that labelled TAIII was internalised in a manner dependent on dynamin. We also found that TAIII blocked internalisation of cell surface proteins including integrin b1. These results provide a novel aspect to understand how TAIII exerts pharmacological activities in suppression of cancer cell migration.

Introduction

Cell motility is closely associated with various physiological processes such as tissue formation and migration during embryonic development, wound healing, and immunological responses. The initial step in motility is the formation of lamellipodia at the leading edge, which is a thin sheet of membrane-enclosed F-actin networks [1]. In accordance with the interaction of lamellipodia with the substrate, cells generate force to start directed movement by translocation of the cell body, followed by retraction of the rear part of the cell [2].

Deregulation of cell motility is involved in pathological events, particularly cancer metastasis [3]. After dissociating from a primary lesion, cancer cells invade through the extracellular matrix (ECM) of their surrounding host tissues and enter blood vessels [4]. In this process, cancer cells communicate with their neighbouring environment, which triggers and promotes invasive properties of cancer cells. Various types of cells, including macrophages and stromal cells, have been reported to be involved in the regulation of cancer cell migration and invasion [5-8]. On the basis of the interactions with the surrounding environment, cancer cells change their morphology and mode of migration. For example, carcinoma cells acquire a mesenchymal-like cell morphology with elongated membrane protrusions, which migrate through surrounding tissues and penetrate the adjacent basement membrane. Therefore, blockade of the morphological plasticity of cancer cells may become a goal of anti-cancer therapies.

Timosaponin AIII (TAIII) is a major steroidal saponin isolated from the root of *Anemarrhena asphodeloides* Bunge [9]. TAIII has multifaceted activities and is traditionally used as an anti-pyretic, anti-inflammatory, anti-diabetic, and anti-coagulant agent in Chinese medicine [10]. It has also been reported that TAIII ameliorates learning and memory deficits in a mouse model [11]. However, the pharmacological

activity of TAIII have been mainly studied in the context of anti-cancer properties in the past decades [10,12]. A major effect of TAIII on cancer cells is cytotoxicity. TAIII causes selective cell death in various kinds of cancer cells at a certain concentration [13-15]. TAIII induces cytochrome c release and caspase activation mediated by overproduction of reactive oxygen species and mitochondrial dysfunction, which lead to apoptosis [16]. Caspase activation followed by poly (ADP)-ribose polymerase cleavage is caused by phosphorylation of JNK and p38 in response to TAIII treatment [17]. TAIII also targets machineries that regulate cell cycle progression in cancer cells, thereby leading to cell cycle arrest in G1 or G2/M phase [13].

Additionally, compelling evidences have demonstrated the inhibitory effects of TAIII on the motility of cancer cells. It has been reported that TAIII regulates proteolytic activity and mRNA expression of matrix metalloproteinase-2/9 [18-21] that play pivotal roles in cell migration and invasion [22,23]. TAIII also contributes to upregulation of microRNAs (miRNAs), which suppresses metastatic properties of cancer cells. In breast cancer cell lines, TAIII induces expression of tumour-suppressive miRNAs miR-200c/141 and reduces expression of its negative regulator, B-cell-specific Moloney murine leukaemia virus integration site 1 [24]. Furthermore, TAIII regulates the expression of miR-129-5p through inhibition of the PI3K/AKT pathway in renal carcinoma cells without altering the viability of cancer cells [25]. Taken together, the anti-metastatic activity of TAIII has been explained by transcriptional control of migration regulatory factors. However, it remains unclear whether TAIII directly controls cellular machineries involved in the generation of migratory force to promote cancer cell invasion and metastasis.

In this study, we found that TAIII disrupted morphological plasticity and migration of breast adenocarcinoma cells promoted by paracrine interactions with mammary epithelial cell lines. TAIII suppressed lamellipodia formation induced by conditioned medium and attenuated membrane ruffling and spreading regulated by exogenously expressed constitutively active forms of Rho family small GTPase Rac1. Interestingly, labelled TAIII was internalised through dynamin-dependent endocytosis pathways and TAIII significantly inhibited internalisation of integrin b1, which downregulated cell adhesion activity on ECM. These findings suggest novel targets of TAIII to inhibit cancer cell motility by the interaction with the surrounding environment.

Materials And Methods

Reagents

The natural compound library was provided by the Cooperative Research Project of the Institute of Natural Medicine, University of Toyama, Japan. TAIII, timosaponin AI (TAI), and timosaponin BIII (TBII) were purchased from Kanto Kagaku (Tokyo, Japan). Anemarrhenasaponin I (AMS) was from MedChemExpress (Monmouth Junction, NJ, USA). Sarsasapogenin was from Fujifilm-Wako Pure Chemicals (Osaka, Japan). Dynasore was from Abcam (Cambridge, UK). Laminin-332, fibronectin, and vitronectin were from ReproCELL (Yokohama, Japan), BD Biosciences (Franklin Lakes, NJ, USA), and Fujifilm-Wako Pure Chemicals, respectively.

To prepare labelled TAIII, Alexa Fluor 568 hydrazide, sodium salt was purchased from Thermo Fisher Scientific (Waltham, MA, USA). Sodium periodate, dichloromethane, chloroform, and methanol were purchased from Fujifilm-Wako Pure Chemicals. All chemicals and reagents obtained from Fujifilm-Wako were guaranteed reagent grade. Spherical silica Chromatorex Q-pack SI 30 size:60 was purchased from Fuji Silysia (Aichi, Japan). ESIMS was measured on a Shimadzu LCmS-2020 system.

Cell culture and transfection

MDA-MB-231 cells (ATCC, Manassas, VA, USA) and HeLa cells (Kyoto) were maintained in Dulbecco's modified Eagle's medium (DMEM) supplemented with 10% fetal bovine serum (FBS). MCF10A cells (ATCC) were cultured in DMEM/F-12 (Thermo Fisher Scientific) supplemented with 5% heat-inactivated horse serum (Thermo Fisher Scientific), 20 ng/mL EGF (Miltenyi Biotec, Bergisch Gladbach, Germany), 10 mg/mL insulin (Sigma-Aldrich, St. Louis, MO, USA), 0.5 mg/mL hydrocortisone (Sigma-Aldrich), and 100 ng/mL cholera toxin (Sigma-Aldrich) at 37°C with 5% CO_2. Preparation and treatment with conditioned medium from MCF10A cells were performed as described previously [26].

For transfection, Lipofectamine LTX (Thermo Fisher Scientific) was used in accordance with the manufacturer's instructions. Expression plasmids for constitutively active Val12 Rac1, Val12 CDC42, and Val14 RhoA have been described previously [26]. The expression plasmid for LifeAct-mCherry was kindly provided by Dr. Naoki Watanabe (Kyoto University) and has been described previously [27].

Scratch wound assay

MDA-MB-231 cells were seeded on 96-well Image-lock plates (Essen Bioscience) in OPTI-MEM (Thermo Fisher Scientific). After incubation overnight, the cells were pretreated with natural compounds at a concentration of 1 mM for 30 min. Then, scratches were made using a 96-pin tool (Woundmaker) in accordance with the manufacturer's instructions, followed by treatment with conditioned medium. The plate was placed in an IncuCyte device and confluence was recorded every 1 h by phase contrast scanning for 8 h at 37°C with 5% CO_2. Images were analysed using IncuCyte ZOOM software. Inhibitory activity of each compound against scratch migration was calculated as the ratio of migration confluence (0 h/8 h) and normalised to the value of DMSO.

Immunofluorescence analyses and time-lapse microscopy

Immunofluorescence analyses were performed as described previously [28] with minor modifications. Cells grown on cover slips were fixed with 4% formaldehyde in phosphate-buffered saline (PBS) containing 0.1% Triton X-100 for 10 min, blocked for 30 min with 2% dry skim milk in PBS, and then incubated for 1 h with a mouse monoclonal anti-vinculin antibody (hVIN-1; Sigma-Aldrich) diluted in blocking buffer. After three times washes with PBS for 5 min each, the cells were incubated for 30 min with Alexa Fluor 488-conjugated anti mouse IgG (Thermo Fisher Scientific) diluted in blocking buffer together with Texas Red™-X Phalloidin (Thermo Fisher Scientific). The cells were then washed with PBS

and mounted, and immunofluorescence was observed under a confocal scanning laser microscope (SP8; Leica). Images were processed using Adobe Photoshop software.

For time-lapse analysis, cells seeded on a 3.5-cm glass-bottom culture dish (Asahi Techno Glass Co., Tokyo, Japan) were observed under the confocal scanning laser microscope equipped with a temperature- and CO_2-controlled stage-top live cell incubator (Tokai Hit, Fujinomiya, Japan).

Migration assay

Cell migration assays were performed in Boyden chambers as described previously [26] with minor modifications. MDA-MB-231 cells were trypsinised, washed twice with OPTI-MEM, and then seeded at 5×10^4 cells per well in OPTI-MEM. MCF10A CM was added to the lower chamber. For TAIII treatments, the inhibitor was added to both upper and lower chambers at the indicated concentrations. After 16 h of incubation, cells that had migrated to the lower surface of the membranes were stained with 0.5% crystal violet in 20% methanol and then counted.

Cell spreading assay

HeLa cells transfected with LifeAct-mCherry-expressing plasmids were trypsinised and washed once with DMEM containing 10% FBS. After incubation for 20 min at 37°C, the cells were seeded on a glass-bottom dish or coverslip coated with fibronectin (10 μg/mL) for time-lapse imaging and immunostaining, respectively. Using the acquired phase contrast images, the cell periphery of more than 100 cells in each condition was drawn and the cell spreading area was measured by ImageJ software.

Adhesion assay

96-well culture plates were coated with 2.5 μg fibronectin, laminin-332, or vitronectin in PBS overnight at 4°C and then blocked with BSA. HeLa cells were trypsinised and washed once with DMEM containing 10% FBS. After incubation for 30 min at 37°C, 8×10^4 cells were plated in each well and incubated for 30 min. The culture plates were washed with PBS to remove unattached cells and then attached cells were fixed with 4% formaldehyde and stained with 5 mg/ml crystal violet for 10 min. After unbound dye was washed away, the cells were lysed with 2% SDS and absorbance at OD 630 was measured.

Integrin internalisation assay

An integrin internalisation assay was performed as reported previously [29] with minor modifications. Briefly, HeLa cells were plated on a fibronectin-coated glass bottom dish and cultured overnight. Surface integrin β1 was labelled with an Alexa Fluor® 488 anti-human integrin β1 antibody (clone TS2/16, Biolegend) at 4°C for 60 min. Then, the cells were incubated at 37°C to allow internalisation. Quantification was performed for one of three representative experiments. Mean pixel intensity from each cell was determined using ImageJ software.

Preparation of Alexa Fluor 568-labelled timosaponin AIII

Water (63 µL), methanol (210 µL), and chloroform (35 µL) were added to a vial that contained TAIII (0.5 mg, 0.67 µmol) and mixed well to a clear solution. Then, a 100 mM aqueous solution of sodium periodate (7 µL, 0.7 µmol) was added to the solution, followed by stirring at room temperature for 30 minutes in the dark. Alexa Fluor 568 hydrazide (0.48 mg, 0.67 µmol) was added to the reaction mixture as a methanol solution (70 µL). After stirring at room temperature for 12 hours in the dark, the solvent was removed under the flow of a nitrogen stream. To the vial containing residue, 4.5 mg silica gel (Chromatorex Q-pack SI 30) suspended in methanol (200 µL) was added and then evaporated to remove the methanol. The obtained residue was suspended in hexane/chloroform (1/1 vol/vol) and loaded onto a silica gel (Chromatorex Q-pack SI 30, 200 mg) column. Products were eluted with methanol/chloroform (1/1 vol/vol) and collected in fractions (0.2 mL each). Fractions 2–7 were combined in a recovering flask, evaporated, and dried under vacuum to produce Alexa Fluor 568-labelled TAIII (0.53 mg, 54% yield) as a dark violet film [ESIMS m/z 1428 (1427.6 calc. for $C72H91N4O22S2^{-}$, M^{-})].

Statistical analysis

Results are presented as the mean ± s.e.m. in Figs. 1d, 2b, 5b, 6c, and 6d and the mean ± s.d. in Figs. 2d and 3d. All statistical analyses were performed using the two-tailed Student's t-test.

Results

TAIII suppresses morphological changes and migration of breast cancer cells induced by paracrine interactions with mammary epithelial cells

In our previous study [26], we demonstrated that conditioned medium from the mammary epithelial cell line MCF10A (MCF10A CM) regulates morphological plasticity and promotes migration of the breast cancer cell line MDA-MB-231. To identify natural compounds with the potential activity to disrupt the responses of breast cancer cells to paracrine interactions with mammary epithelial cells, we screened a natural compound library by a scratch wound assay. MDA-MB-231 cells were plated under a serum-deprived condition and treated with each natural compound at a concentration of 1 mM and MCF10A CM (Fig. 1a). As we reported previously [26], baicalein suppressed migration of MDA-MB-231 cells induced by MCF10A CM (Fig. 1b). Although saikosaponin a and d clearly suppressed migration of MDA-MB-231 cells, they also induced cell death during the assays (Fig. 1b). Among the compounds that inhibited migration of MDA-MB-231 cells, TAIII exhibited the strongest activity without cytotoxicity (Fig. 1b and c). The effect of TAIII in conditioned medium-induced migration was confirmed using a Boyden chamber (Fig. 1d). Therefore, we further analysed the effects of TAIII on breast cancer cell migration regulated by paracrine interactions.

First, we examined whether TAIII disrupted the morphological plasticity of breast adenocarcinoma cells regulated by conditioned medium from mammary epithelial cells. We treated MDA-MB-231 cells with MCF10A CM in the presence of TAIII for 1 h and then observed their morphology. As shown in Fig. 2a, MDA-MB-231 cells became elongated and changed their morphology in response to MCF10A CM.

However, MCF10A CM-induced morphological changes were perturbed in the presence of TAIII (Fig. 2a). These effects of TAIII were confirmed by quantification of the cell length (Fig. 2b).

Upon MCF10A CM treatment, MDA-MB-231 cells spread and formed lamellipodia at their leading edge and started migration (Fig. 2c and d, and Supplementary Video 1). Thus, we addressed whether TAIII also influenced lamellipodia formation. Time-lapse imaging analysis revealed that TAIII-treated cells did not extend lamellipodia in response to MCF10A CM. The ratio of the lamellipodia area induced by MCF10A CM in TAIII-treated cells was significantly lower than that in control cells (Fig. 2c–e and Supplementary Video 2). These results suggested that TAIII inhibited lamellipodia formation, thereby suppressing morphological plasticity and migration of breast adenocarcinoma cells induced by paracrine interactions with mammary epithelium-derived cells.

Because TAIII suppressed lamellipodia formation upon treatment with MCF10A CM, we next examined whether TAIII also affected lamellipodia formation induced by serum. MDA-MB-231 cells in normal culture medium were treated with TAIII and their morphology was observed. In this experiment, we treated cells with TAIII at a concentration of 10 mM because we did not observe any effects of TAIII at the lower concentration, which was probably due to the presence of protein components in serum, such as albumins and lipoproteins. Time-lapse analysis by phase contrast microscopy revealed that TAIII treatment disrupted lamellipodia formation (Supplementary Fig. S1a and b, and Supplementary Video 3). The number of cells with membrane ruffling was immediately and significantly decreased up to 10 min (10.8±3.79%) and then temporary recovered at 20 min (34.7±1.52%) but decreased again at 60 min (7.88±1.21%) after treatment (Supplementary Fig. S1c). The lamellipodia area in each cell upon TAIII treatment showed similar changes (Supplementary Fig. S1d). Accordingly, the sizes of MDA-MB-231 cells became significantly smaller by approximately 50% after TAIII treatment (Supplementary Fig. S1e). Fluorescence imaging analysis revealed that actin-rich structures at the leading edge had disappeared in MDA-MB-231 cells treated with TAIII (Supplementary Fig. S1f). Together with the data from Fig. 2, TAIII negatively regulated lamellipodia formation induced by extracellular stimuli.

We also treated epidermoid carcinoma A431 cells with TAIII and observed their membrane dynamics. In the presence of serum, A431 cells tightly associated with each other and exhibited expanded lamellipodia in the cell edge and collective migration (Supplementary Fig. S2 and Video 4). However, lamellipodia formation had disappeared and migratory activity was apparently suppressed in TAIII-treated cells, while their cell-cell interactions shown by E-cadherin staining appeared intact (Supplementary Fig. S2 and Supplementary Video 5). These results corroborated the observations in breast adenocarcinoma cells that TAIII exerted inhibitory effects on cell migration by disrupting lamellipodia formation.

TAIII attenuates membrane dynamics regulated by Rac

To further investigate the effect of TAIII on membrane dynamics, we next accessed the effect of TAIII on cell spreading onto ECM. HeLa cells were transfected with the expression plasmid for LifeAct-mCherry, a widely used actin-binding peptide fused to mCherry protein [30], and replated onto a fibronectin-coated glass bottom dish. When the cells had attached to the glass-bottom dish, we treated them with TAIII and

examined their behaviours by time-lapse microscopy (Fig. 3a). After attachment to fibronectin, DMSO-treated cells showed membrane blebbing and then formed membrane ruffling and protrusions, followed by rapid spreading to the largest extension (Fig. 3b and Supplementary Video 6). We also observed dynamic remodelling of the actin cytoskeleton in response to the interaction with fibronectin (Fig. 3b and Supplementary Video 6). Moreover, vinculin-positive structures were scattered in the cell edge (Fig. 3c). Conversely, TAIII-treated cells did not form membrane blebs or ruffling. They adhered to the culture dish after replating and formed filopodia-like protrusions but could not spread on the dish (Fig. 3b and Supplementary Video 7). Vinculin-positive structures in TAIII-treated cells were obviously tiny compared with those in DMSO-treated cells (Fig. 3c). Accordingly, the cell area of TAIII-treated cells became significantly smaller, which was dependent on the dose of TAIII (Fig. 3d). These results demonstrated the specific activity of TAIII in the regulation of membrane dynamics, which is important for cell spreading.

Because it is well-known that lamellipodia formation and membrane ruffling is regulated by activated Rac, a Rho family GTPase [31], we addressed whether TAIII influenced activation of Rac. To this end, we first transfected HeLa cells with expression plasmids for green fluorescent protein (GFP) and LifeAct-mCherry and then subjected them to time-lapse imaging analyses (Fig. 4a). As shown by fluorescence signals, HeLa cells continuously formed membrane protrusions and showed ruffling under normal culture conditions (Fig. 4b and Supplementary Videos 8 and 9). However, similar to the other cultured cells examined in this study, these membrane dynamics were suppressed by 60 min of TAIII treatment, followed by expansion of intercellular gaps (Fig. 4b and Supplementary Videos 8 and 9). We also confirmed attenuation of membrane dynamics in response to TAIII treatment by kymograph analysis (Fig. 4b). We next examined membrane and actin cytoskeleton dynamics upon TAIII treatment in HeLa cells that overexpressed GFP-tagged constitutively activated Rac1 (GFP-Val12 Rac1) together with LifeAct-mCherry. Overexpression of GFP-Val12 Rac1 induced cell spreading and frequent membrane ruffling, followed by drastic remodelling of the actin cytoskeleton at the cell edge (Fig. 4c and Supplementary Videos 10 and 11). Interestingly, upon TAIII treatment, membrane ruffling was immediately attenuated and cell contraction was observed (Fig. 4c and Supplementary Videos 10 and 11). The rapid changes of membrane dynamics in Val12 Rac1-expressing cells induced by TAIII treatment were also shown by kymograph analysis (Fig. 4c). These data demonstrated that TAIII controlled membrane ruffling independently of the regulation of Rac activity. We also examined the effects of TAIII on filopodia formation and actin stress fibres regulated by constitutively active CDC42 (Val12 CDC42) and RhoA (Val14 RhoA), respectively. Unlike Val12 Rac1-expressing cells, Val12 CDC42- and Val14 RhoA-expressing cells retained membrane and actin cytoskeleton dynamics even after TAIII treatment (Supplementary Fig. S3 and Supplementary Videos 12–15), which implied that TAIII specifically inhibited membrane dynamics regulated by Rac signalling.

Immunofluorescence analysis revealed that HeLa cells treated with TAIII also showed morphological changes with accumulation of vinculin-positive structures at the cell edge and expanded intercellular gaps (Supplementary Fig. S4). Therefore, we also assessed the structure-activity relationship among saponins isolated from the rhizome of *Anemarrhena asphodeloides* in the regulation of membrane dynamics (Supplementary Fig. S4a). TAI is a deglycosylated derivative of TAIII, which lacks glucose in its

saccharide moiety. TBII and AMS share the steroid core and disaccharide moiety that are identical to those of TAIII. TBII contains an extra sugar moiety at the end of the steroidal side chain. However, AMS does not harbour additional sugar moieties, whereas a hydroxyl group is linked to the C-15 position in its steroid core. We found that HeLa cells treated with these TAIII derivatives did not show any obvious morphological changes similar to those observed after treatment with TAIII (Supplementary Fig. S4b). We also examined sarsasapogenin, an aglycone of TAIII, and found that it had no significant effects on cell morphology or vinculin localisation (Supplementary Fig. S4b). We further tested the natural compound library to determine whether it contained inhibitory activities in the regulation of membrane dynamics. Among the compounds in the library, only shikonin and alkannin affected the morphology of HeLa cells. The cells treated with these compounds became rounded and detached from the culture dish upon treatment, probably because of their cytotoxicity (Supplementary Table S1). Triterpenoid saponins, such as astragaloside IV, ginsenosides (Rb1, Rc, Rd, Re, and Rg1), glycyrrhizic acid, and saikosaponins (a, b2, c, and d), and cardiotonic steroid bufadienolides, such as bufalin and bufotalin (Supplementary Table S1), are listed in the library. However, unlike TAIII, these compounds did not exert any obvious effects on cell morphology. Collectively, these results supported the unique activity of TAIII in the regulation of membrane ruffling.

TAIII inhibits integrin internalisation

We next clarified the mechanisms underlying how TAIII suppressed membrane ruffling. To this end, we labelled TAIII with a fluorescence dye, Alexa Fluor 568, in accordance with the results from the structure-activity relationship among TAIII derivatives and examined its intracellular behaviour. Time-lapse analysis revealed that, after attachment to the plasma membrane, labelled TAIII formed intracellular vesicle-like structures and accumulated in cytoplasm (Fig. 5a and b, and Supplementary Video 16). Intriguingly, these intracellular vesicles and accumulation of labelled TAIII were less observed when cells were pretreated with a dynamin inhibitor, dynasore [32] (Fig. 5a and b, and Supplementary Video 17), which suggested that TAIII was internalised through a dynamin-dependent pathway.

Considering the observation that TAIII was internalised through dynamin-dependent endocytic pathways (Fig. 5), we focused on endocytic trafficking of cell surface proteins. In particular, we examined behaviours of integrin b1 in response to TAIII treatment (Fig. 6a) because TAIII-treated cells showed impaired formation of adhesion complexes positive for vinculin during spreading on fibronectin (Fig. 3c). Cell surface integrin b1 was labelled on ice with an Alexa Fluor 488-conjugated antibody, allowed to internalise at 37°C, and then subjected to time-lapse imaging analysis. Intracellular fluorescence signals from traced integrin b1, which was transported via endosomes on the basis of their estimated size (0.5–2 mm) [29], were observed in cells treated with DMSO up to 20 min after incubation at 37°C and its fluorescence intensity was increased over time (Fig. 6b and c, and Supplementary Videos 18 and 19). Conversely, we did not detect any intracellular signals of internalised integrin β1 in TAIII-treated cells after incubation at 37°C, in which fluorescent signals of LifeAct-mCherry indicated cell contraction, although signals from labelled integrin traced cell shapes prior to TAIII treatment (Fig. 6b and c, and Supplementary Videos 20 and 21). Interestingly, internalisation of integrin β1 was clearly suppressed, whereas

continuous internalisation and intracellular accumulation of labelled TAIII were observed (Supplementary Fig. S5 and Supplementary Videos 22 and 23). We next examined the intracellular dynamics of integrin b1 and TAIII. We labelled cell surface integrin b1 and incubated the cells at 37°C for 1 h to allow internalisation and then treated the cells with labelled TAIII (Supplementary Fig. S6a). Whereas any colocalisation signals were not observed on the cell surface, some internalised integrin b1 and TAIII had merged in the cytoplasm (Supplementary Fig. S6b and Supplementary Videos 24–26). We also found that TAIII suppressed internalisation of E-cadherin induced by EGTA in A431 cells (Supplementary Fig. S7). Collectively, these results suggested that TAIII inhibited machineries that regulated internalisation of specific cargo proteins such as integrin b1.

To further elucidate the effect of TAIII on integrin mediated cell functions, we performed cell adhesion assays with various ECM proteins. Trypsinised HeLa cells were treated with TAIII for 30 min and replated on culture dishes coated with each ECM protein. After incubation for another 30 min, cells associated with the ECM were measured. We examined purified fibronectin, laminin-332, and vitronectin that serve as ligands for integrins a5b1, a3b1, and avb1, respectively, which are expressed in HeLa cells [33]. Adhesion assays revealed that TAIII significantly interfered with the substantial interaction of HeLa cells with purified integrin ligands in a dose-dependent manner (Fig. 6d), which demonstrated that TAIII targeted integrin heterodimers consisting of at least integrin b1. Thus, the results suggested that the effect of TAIII on the regulation of internalisation of cell surface proteins, such as integrin b1, contributed in part to its inhibitory activity against cell migration through suppression of lamellipodia formation and membrane ruffling.

Discussion

In this study, we found that TAIII exerted a strong suppressive effect on the migration of breast adenocarcinoma cells by paracrine interactions with mammary epithelium-derived cells. Lamellipodia formation and membrane ruffling induced by conditioned medium from mammary epithelial cells were clearly disrupted by TAIII. TAIII inhibited internalisation of cell surface proteins, including integrin b1, which explains its inhibitory activity against lamellipodia formation and cell migration. The overall mechanisms of TAIII in the regulation of cell motility have not been determined completely. Our study provides a novel aspect to understand how TAIII exerts anti-metastatic effects.

Moreover, we investigated intracellular behaviours of TAIII using fluorescent labelling techniques. Fluorescent labelling is a powerful strategy to perform high-resolution imaging analysis of target molecules. Indeed, fluorescent dye-labelled analogues have been used to examine intracellular localisation and trafficking of cholesterols [34]. However, labelling strategies have not been applied to saponins because the biological activities, including cytotoxicity, of saponins are closely associated with their aglycone moieties and the number and structures of monosaccharides in their sugar chains [35]. In accordance with the results from the examination of the structure-activity relationships among TAIII derivatives, we modified TAIII and evaluated intracellular behaviours of labelled TAIII. To our knowledge, this is a first report to reveal the intracellular dynamics of TAIII. The data obtained using labelled TAIII

revealed a novel function of TAIII as a negative regulator of endocytic trafficking. This would be a great benefit to address intracellular behaviours of natural compounds, which led us to elucidate their molecular functions and properly understand their pharmacological properties.

A shift in migration modes allows cancer cells to adapt and invade into their surrounding tissues. Paracrine interactions with the microenvironment play pivotal roles in regulating the changes in migration mode, such as epithelial-mesenchymal transition. To date, various factors such as the ECM and chemokines have been reported to have tumour-promoting properties [36,37]. We found that TAIII suppressed morphological plasticity and migration of breast adenocarcinoma cells induced by conditioned medium from mammary epithelial cells. The activity of conditioned medium from mammary epithelial cells is mainly mediated by secreted laminin-332 [26]. Laminins are a component in the basement membrane of mammary ducts and secreted from myoepithelial cells [7]. In particular, laminin-332 plays critical roles in regulating the motility of breast cancer cells [38,39]. Clinical investigations have demonstrated that laminin-332 is enriched in the invasion interface of breast-invasive ductal carcinoma [39]. Additionally, the expression level of laminins is significantly associated with distant metastasis-free survival of patients with breast cancers at the early stage [40]. Therefore, our observations support development of TAIII as an anti-cancer drug to suppress cancer cell metastasis and invasion dependent on the microenvironment.

Interestingly, TAIII disrupted membrane dynamics by inducing overexpression of constitutively active Rac1, but not other Rho family GTPases, in HeLa cells. These observations suggest that TAIII targets downstream of Rac, such as WAVE2 and IRSp53 [41-43], to suppress lamellipodia formation and membrane ruffling. However, our data demonstrated the inhibitory effects of TAIII on internalisation of cell surface proteins including integrin b1 and integrin-mediated cell adhesion. Integrin heterodimers play a crucial role in formation of adhesion complexes that serve as platforms to induce lamellipodia formation and promote cell migration [44]. Integrins are also required to stabilise lamellipodia formation [45]. The spatiotemporal regulation of cell surface integrins through trafficking systems gives impact to their functions in the context of cell migration [46-50]. Furthermore, a ligand of integrin heterodimers, laminin-332, plays important roles in the regulation of morphological plasticity and cell migration of MDA-MB-231 cells [26]. Collectively, our results lead us to propose that the activity of TAIII to block internalisation of integrin b1 should contribute, in part, to its inhibitory effect on cell migration through negative regulation of lamellipodia formation. This conclusion is consistent with a previous observation that demonstrated the importance of endocytosis to regulate lamellipodia formation and cancer cell invasion [51].

A recent study has demonstrated that TAIII inhibits platelet aggregation induced by U46619 *in vitro* and prevents thrombus formation *in vivo* [52]. Anti-platelet and anti-thrombotic activities of TAIII are reported to be mediated by decreased adenosine diphosphate (ADP) secretion caused by suppression of thromboxane A2 receptor activity and the Gq signalling pathway. Apart from the suppression of ADP secretion, blockade of integrin activation is an important strategy to interfere with platelet crosslinking and platelet-derived thrombus formation. In fact, inhibitors of glycoprotein IIb/IIIa, an integrin complex on

platelets, such as abciximab, eptifibatide, and tirofiban, are used clinically [53]. Therefore, we speculate that the anti-platelet and anti-thrombotic activity of TAIII might, in part, be also mediated by the negative regulation of integrin internalisation. TAIII also exerts anti-angiogenesis effects through inactivation of VEGF signalling [15]. Receptor internalisation and subsequent cytoplasmic trafficking are required for activation of signalling cascades mediated by proangiogenic growth factors in endothelial cells *in vitro* and *in vivo* [54]. Our observations might also explain the pharmacological activity of TAIII in the context of endocytic regulation of signal transduction.

We found suppression of integrin b1 internalisation induced by TAIII regardless of continuous intracellular accumulation of TAIII itself, which demonstrated that TAIII regulated endocytosis of a specific subclass of cargoes. Additionally, this result also raised a question how TAIII regulated internalisation of cell surface proteins. TAIII is considered to direct membrane-associating proteins in accordance with computational docking approaches demonstrating that TAIII would associate with the receptor for advanced glycation end products (RAGE) to modulate RAGE/MAPK signalling pathways [55]. Furthermore, cardiac glycosides, digoxin, and oubain bind to cell surface Na+,K+-ATPase to exert its enzymatic activity [56]. Therefore, TAIII might interact with its membrane targets to regulate internalisation of cargo proteins. However, in this study, we did not observe clear colocalised signals of labelled TAIII and integrin b1 at the plasma membrane. It has been reported that abrogation of the recycling pathway impairs integrin internalisation and downregulation of migratory activity [29]. Taken together with our observation that labelled TAIII colocalised with integrin b1 in intracellular vesicles of cells treated with labelled TAIII after internalisation of integrin β1 was allowed, TAIII might disrupt the regulatory machineries for trafficking vesicles, thereby suppressing internalisation of cell surface cargoes. More than two decades, numerous efforts were made to reveal the overall network of integrin trafficking and various membrane-associating proteins were found to be involved in integrin trafficking [29,57]. It would also be interesting to explore the molecular targets of TAIII, which might expand our knowledge of the regulatory machineries for cargo transport.

Herbal medicines have been used as therapies against various diseases. While numerous compounds have been isolated, little is known about how these compounds exert their fascinating pharmacological effects. In this study, we uncovered the activity of TAIII in suppression of lamellipodia formation and migration of breast cancer cells, which would be mediated, in part, through blocking internalisation of cell surface proteins including integrin. However, it remains unresolved how TAIII blocks internalisation of cell surface proteins. Further studies are needed to clarify the mechanisms underlying the regulation of internalisation by TAIII, which would contribute to re-evaluating traditional medicines for drug development.

Abbreviations

AMS: Anemarrhenasaponin I

CM: Conditioned medium

ECM: Extracellular matrix

GFP: Green fluorescent protein

miRNAs: microRNAs

RAGE: Receptor for advanced glycation end products

TAIII: Timosaponin AIII

TBII: Timosaponin BII

Declarations

Ethics declarations

Funding

JSPS KAKENHI (17K08339) for Toshimasa Ishizaki

JSPS KAKENHI (19K08776) for Takeshi Terabayashi

Conflicts of interest/Competing interests

We have no conflicts of interest or competing interests.

Availability of data and material

It can be supplied if necessary.

Code availability

IncuCyte ZOOM software and Adobe Photoshop software are licensed. ImageJ is opensource software.

Ethics approval and consent to participate

Not applicable

Consent for publication

Not applicable

Authors' contributions

T.T. and T.I. conceived the study design. T.T., K.H., and T.I. performed the experiments and analyzed the data, with contributions from T.A.. S.M., T.S., and A.K. produced materials for the experiments. T.T wrote

the manuscript, with contributions from K.H., T.S. and T.I.. All the authors have read and confirmed the final version of the manuscript.

Acknowledgements

We would like to thank Dr. Naoki Watanabe, Kyoto University, for a kind gift of plasmid for LifeAct-mCherry. We also like to thank Mitchell Arico from Edanz Group (https://en-author-services.edanz.com/ac) for editing a draft of this manuscript. This study was supported by JSPS KAKENHI Grant Number 17K08339 for T.I. and 19K08776 for T.T., and was performed as a part of the Cooperative Research Project with Institute of Natural Medicine, University of Toyama in 2017.

References

1. Krause M, Gautreau A (2014) Steering cell migration: lamellipodium dynamics and the regulation of directional persistence. Nat Rev Mol Cell Biol 15 (9):577-590. doi:10.1038/nrm3861
2. Pollard TD, Borisy GG (2003) Cellular motility driven by assembly and disassembly of actin filaments. Cell 112 (4):453-465. doi:10.1016/s0092-8674(03)00120-x
3. Bravo-Cordero JJ, Hodgson L, Condeelis J (2012) Directed cell invasion and migration during metastasis. Curr Opin Cell Biol 24 (2):277-283. doi:10.1016/j.ceb.2011.12.004
4. Friedl P, Alexander S (2011) Cancer invasion and the microenvironment: plasticity and reciprocity. Cell 147 (5):992-1009. doi:10.1016/j.cell.2011.11.016
5. Qian BZ, Pollard JW (2010) Macrophage diversity enhances tumor progression and metastasis. Cell 141 (1):39-51. doi:10.1016/j.cell.2010.03.014
6. Gascard P, Tlsty TD (2016) Carcinoma-associated fibroblasts: orchestrating the composition of malignancy. Genes Dev 30 (9):1002-1019. doi:10.1101/gad.279737.116
7. Hu M, Yao J, Carroll DK, Weremowicz S, Chen H, Carrasco D, Richardson A, Violette S, Nikolskaya T, Nikolsky Y, Bauerlein EL, Hahn WC, Gelman RS, Allred C, Bissell MJ, Schnitt S, Polyak K (2008) Regulation of in situ to invasive breast carcinoma transition. Cancer Cell 13 (5):394-406. doi:10.1016/j.ccr.2008.03.007
8. Sanz-Moreno V, Gaggioli C, Yeo M, Albrengues J, Wallberg F, Viros A, Hooper S, Mitter R, Feral CC, Cook M, Larkin J, Marais R, Meneguzzi G, Sahai E, Marshall CJ (2011) ROCK and JAK1 signaling cooperate to control actomyosin contractility in tumor cells and stroma. Cancer Cell 20 (2):229-245. doi:10.1016/j.ccr.2011.06.018
9. Wang Y, Dan Y, Yang D, Hu Y, Zhang L, Zhang C, Zhu H, Cui Z, Li M, Liu Y (2014) The genus Anemarrhena Bunge: A review on ethnopharmacology, phytochemistry and pharmacology. J Ethnopharmacol 153 (1):42-60. doi:10.1016/j.jep.2014.02.013
10. Lin Y, Zhao WR, Shi WT, Zhang J, Zhang KY, Ding Q, Chen XL, Tang JY, Zhou ZY (2020) Pharmacological Activity, Pharmacokinetics, and Toxicity of Timosaponin AIII, a Natural Product

Isolated From Anemarrhena asphodeloides Bunge: A Review. Front Pharmacol 11:764. doi:10.3389/fphar.2020.00764

11. Lee B, Jung K, Kim DH (2009) Timosaponin AIII, a saponin isolated from Anemarrhena asphodeloides, ameliorates learning and memory deficits in mice. Pharmacol Biochem Behav 93 (2):121-127. doi:10.1016/j.pbb.2009.04.021
12. Han FY, Song XY, Chen JJ, Yao GD, Song SJ (2018) Timosaponin AIII: A novel potential anti-tumor compound from Anemarrhena asphodeloides. Steroids 140:125-130. doi:10.1016/j.steroids.2018.09.014
13. Kang YJ, Chung HJ, Nam JW, Park HJ, Seo EK, Kim YS, Lee D, Lee SK (2011) Cytotoxic and antineoplastic activity of timosaponin A-III for human colon cancer cells. J Nat Prod 74 (4):701-706. doi:10.1021/np1007735
14. Wang N, Feng Y, Zhu M, Siu FM, Ng KM, Che CM (2013) A novel mechanism of XIAP degradation induced by timosaponin AIII in hepatocellular carcinoma. Biochim Biophys Acta 1833 (12):2890-2899. doi:10.1016/j.bbamcr.2013.07.018
15. Zhou ZY, Zhao WR, Xiao Y, Zhou XM, Huang C, Shi WT, Zhang J, Ye Q, Chen XL, Tang JY (2020) Antiangiogenesis effect of timosaponin AIII on HUVECs in vitro and zebrafish embryos in vivo. Acta Pharmacol Sin 41 (2):260-269. doi:10.1038/s41401-019-0291-z
16. Sy LK, Yan SC, Lok CN, Man RY, Che CM (2008) Timosaponin A-III induces autophagy preceding mitochondria-mediated apoptosis in HeLa cancer cells. Cancer Res 68 (24):10229-10237. doi:10.1158/0008-5472.CAN-08-1983
17. Huang HL, Chiang WL, Hsiao PC, Chien MH, Chen HY, Weng WC, Hsieh MJ, Yang SF (2015) Timosaponin AIII mediates caspase activation and induces apoptosis through JNK1/2 pathway in human promyelocytic leukemia cells. Tumour Biol 36 (5):3489-3497. doi:10.1007/s13277-014-2985-7
18. Tsai CH, Yang CW, Wang JY, Tsai YF, Tseng LM, King KL, Chen WS, Chiu JH, Shyr YM (2013) Timosaponin AIII Suppresses Hepatocyte Growth Factor-Induced Invasive Activity through Sustained ERK Activation in Breast Cancer MDA-MB-231 Cells. Evid Based Complement Alternat Med 2013:421051. doi:10.1155/2013/421051
19. Jung O, Lee J, Lee YJ, Yun JM, Son YJ, Cho JY, Ryou C, Lee SY (2016) Timosaponin AIII inhibits migration and invasion of A549 human non-small-cell lung cancer cells via attenuations of MMP-2 and MMP-9 by inhibitions of ERK1/2, Src/FAK and beta-catenin signaling pathways. Bioorg Med Chem Lett 26 (16):3963-3967. doi:10.1016/j.bmcl.2016.07.004
20. Jung O, Lee SY (2019) Synergistic anticancer effects of timosaponin AIII and ginsenosides in MG63 human osteosarcoma cells. J Ginseng Res 43 (3):488-495. doi:10.1016/j.jgr.2018.11.002
21. Kim Y, Kim KH, Lee IS, Park JY, Na YC, Chung WS, Jang HJ (2019) Apoptosis and G2/M cell cycle arrest induced by a timosaponin A3 from Anemarrhena asphodeloides Bunge on AsPC-1 pancreatic cancer cells. Phytomedicine 56:48-56. doi:10.1016/j.phymed.2018.08.006

22. Shay G, Lynch CC, Fingleton B (2015) Moving targets: Emerging roles for MMPs in cancer progression and metastasis. Matrix Biol 44-46:200-206. doi:10.1016/j.matbio.2015.01.019
23. Lyu Y, Xiao Q, Yin L, Yang L, He W (2019) Potent delivery of an MMP inhibitor to the tumor microenvironment with thermosensitive liposomes for the suppression of metastasis and angiogenesis. Signal Transduct Target Ther 4 (1):26. doi:10.1038/s41392-019-0054-9
24. Gergely JE, Dorsey AE, Dimri GP, Dimri M (2018) Timosaponin A-III inhibits oncogenic phenotype via regulation of PcG protein BMI1 in breast cancer cells. Mol Carcinog 57 (7):831-841. doi:10.1002/mc.22804
25. Chiang KC, Lai CY, Chiou HL, Lin CL, Chen YS, Kao SH, Hsieh YH (2019) Timosaponin AIII inhibits metastasis of renal carcinoma cells through suppressing cathepsin C expression by AKT/miR-129-5p axis. J Cell Physiol 234 (8):13332-13341. doi:10.1002/jcp.28010
26. Terabayashi T, Hanada K, Motani K, Kosako H, Yamaoka M, Kimura T, Ishizaki T (2018) Baicalein disturbs the morphological plasticity and motility of breast adenocarcinoma cells depending on the tumor microenvironment. Genes Cells 23 (6):466-479. doi:10.1111/gtc.12584
27. Higashida C, Kiuchi T, Akiba Y, Mizuno H, Maruoka M, Narumiya S, Mizuno K, Watanabe N (2013) F- and G-actin homeostasis regulates mechanosensitive actin nucleation by formins. Nat Cell Biol 15 (4):395-405. doi:10.1038/ncb2693
28. Terabayashi T, Sakaguchi M, Shinmyozu K, Ohshima T, Johjima A, Ogura T, Miki H, Nishinakamura R (2012) Phosphorylation of Kif26b promotes its polyubiquitination and subsequent proteasomal degradation during kidney development. PLoS One 7 (6):e39714. doi:10.1371/journal.pone.0039714
29. Saez-Ibanez AR, Scheffler JM, Terabayashi T, Daubel N, Makinen T, Idevall-Hagren O, Ferby I (2020) Ligand-independent role of ErbB3 in endocytic recycling. bioRxiv:575449. doi:10.1101/575449
30. Riedl J, Crevenna AH, Kessenbrock K, Yu JH, Neukirchen D, Bista M, Bradke F, Jenne D, Holak TA, Werb Z, Sixt M, Wedlich-Soldner R (2008) Lifeact: a versatile marker to visualize F-actin. Nat Methods 5 (7):605-607. doi:10.1038/nmeth.1220
31. Ridley AJ, Paterson HF, Johnston CL, Diekmann D, Hall A (1992) The small GTP-binding protein rac regulates growth factor-induced membrane ruffling. Cell 70 (3):401-410. doi:10.1016/0092-8674(92)90164-8
32. Macia E, Ehrlich M, Massol R, Boucrot E, Brunner C, Kirchhausen T (2006) Dynasore, a cell-permeable inhibitor of dynamin. Dev Cell 10 (6):839-850. doi:10.1016/j.devcel.2006.04.002
33. Maginnis MS, Forrest JC, Kopecky-Bromberg SA, Dickeson SK, Santoro SA, Zutter MM, Nemerow GR, Bergelson JM, Dermody TS (2006) Beta1 integrin mediates internalization of mammalian reovirus. J Virol 80 (6):2760-2770. doi:10.1128/JVI.80.6.2760-2770.2006
34. Kralova J, Jurasek M, Miksatkova L, Maresova A, Fahnrich J, Cihlarova P, Drasar P, Bartunek P, Kral V (2020) Influence of fluorophore and linker length on the localization and trafficking of fluorescent sterol probes. Sci Rep 10 (1):22053. doi:10.1038/s41598-020-78085-9
35. Podolak I, Galanty A, Sobolewska D (2010) Saponins as cytotoxic agents: a review. Phytochem Rev 9 (3):425-474. doi:10.1007/s11101-010-9183-z

36. Nagarsheth N, Wicha MS, Zou W (2017) Chemokines in the cancer microenvironment and their relevance in cancer immunotherapy. Nat Rev Immunol 17 (9):559-572. doi:10.1038/nri.2017.49
37. Winkler J, Abisoye-Ogunniyan A, Metcalf KJ, Werb Z (2020) Concepts of extracellular matrix remodelling in tumour progression and metastasis. Nat Commun 11 (1):5120. doi:10.1038/s41467-020-18794-x
38. Carpenter PM, Dao AV, Arain ZS, Chang MK, Nguyen HP, Arain S, Wang-Rodriguez J, Kwon SY, Wilczynski SP (2009) Motility induction in breast carcinoma by mammary epithelial laminin 332 (laminin 5). Mol Cancer Res 7 (4):462-475. doi:10.1158/1541-7786.MCR-08-0148
39. Kim BG, An HJ, Kang S, Choi YP, Gao MQ, Park H, Cho NH (2011) Laminin-332-rich tumor microenvironment for tumor invasion in the interface zone of breast cancer. Am J Pathol 178 (1):373-381. doi:10.1016/j.ajpath.2010.11.028
40. Lee MH, Wu PH, Gilkes D, Aifuwa I, Wirtz D (2015) Normal mammary epithelial cells promote carcinoma basement membrane invasion by inducing microtubule-rich protrusions. Oncotarget 6 (32):32634-32645
41. Takenawa T, Miki H (2001) WASP and WAVE family proteins: key molecules for rapid rearrangement of cortical actin filaments and cell movement. J Cell Sci 114 (Pt 10):1801-1809
42. Abou-Kheir W, Isaac B, Yamaguchi H, Cox D (2008) Membrane targeting of WAVE2 is not sufficient for WAVE2-dependent actin polymerization: a role for IRSp53 in mediating the interaction between Rac and WAVE2. J Cell Sci 121 (Pt 3):379-390. doi:10.1242/jcs.010272
43. Lee SH, Dominguez R (2010) Regulation of actin cytoskeleton dynamics in cells. Mol Cells 29 (4):311-325. doi:10.1007/s10059-010-0053-8
44. Ridley AJ, Schwartz MA, Burridge K, Firtel RA, Ginsberg MH, Borisy G, Parsons JT, Horwitz AR (2003) Cell migration: integrating signals from front to back. Science 302 (5651):1704-1709. doi:10.1126/science.1092053
45. Choma DP, Pumiglia K, DiPersio CM (2004) Integrin alpha3beta1 directs the stabilization of a polarized lamellipodium in epithelial cells through activation of Rac1. J Cell Sci 117 (Pt 17):3947-3959. doi:10.1242/jcs.01251
46. Caswell PT, Norman JC (2006) Integrin trafficking and the control of cell migration. Traffic 7 (1):14-21. doi:10.1111/j.1600-0854.2005.00362.x
47. Pellinen T, Ivaska J (2006) Integrin traffic. J Cell Sci 119 (Pt 18):3723-3731. doi:10.1242/jcs.03216
48. Bridgewater RE, Norman JC, Caswell PT (2012) Integrin trafficking at a glance. J Cell Sci 125 (Pt 16):3695-3701. doi:10.1242/jcs.095810
49. De Franceschi N, Hamidi H, Alanko J, Sahgal P, Ivaska J (2015) Integrin traffic - the update. J Cell Sci 128 (5):839-852. doi:10.1242/jcs.161653
50. Paul NR, Jacquemet G, Caswell PT (2015) Endocytic Trafficking of Integrins in Cell Migration. Curr Biol 25 (22):R1092-1105. doi:10.1016/j.cub.2015.09.049

51. Yamada H, Abe T, Li SA, Masuoka Y, Isoda M, Watanabe M, Nasu Y, Kumon H, Asai A, Takei K (2009) Dynasore, a dynamin inhibitor, suppresses lamellipodia formation and cancer cell invasion by destabilizing actin filaments. Biochem Biophys Res Commun 390 (4):1142-1148. doi:10.1016/j.bbrc.2009.10.105
52. Cong Y, Wang L, Peng R, Zhao Y, Bai F, Yang C, Liu X, Wang D, Ma B, Cong Y (2016) Timosaponin AIII induces antiplatelet and antithrombotic activity via Gq-mediated signaling by the thromboxane A2 receptor. Sci Rep 6:38757. doi:10.1038/srep38757
53. Bledzka K, Smyth SS, Plow EF (2013) Integrin alphaIIbbeta3: from discovery to efficacious therapeutic target. Circ Res 112 (8):1189-1200. doi:10.1161/CIRCRESAHA.112.300570
54. Simons M, Gordon E, Claesson-Welsh L (2016) Mechanisms and regulation of endothelial VEGF receptor signalling. Nat Rev Mol Cell Biol 17 (10):611-625. doi:10.1038/nrm.2016.87
55. Wang N, Xu P, Wang X, Yao W, Wang B, Wu Y, Shou D (2020) Timosaponin AIII attenuates inflammatory injury in AGEs-induced osteoblast and alloxan-induced diabetic osteoporosis zebrafish by modulating the RAGE/MAPK signaling pathways. Phytomedicine 75:153247. doi:10.1016/j.phymed.2020.153247
56. Laursen M, Gregersen JL, Yatime L, Nissen P, Fedosova NU (2015) Structures and characterization of digoxin- and bufalin-bound Na+,K+-ATPase compared with the ouabain-bound complex. Proc Natl Acad Sci U S A 112 (6):1755-1760. doi:10.1073/pnas.1422997112
57. Moreno-Layseca P, Icha J, Hamidi H, Ivaska J (2019) Integrin trafficking in cells and tissues. Nat Cell Biol 21 (2):122-132. doi:10.1038/s41556-018-0223-z

Figures

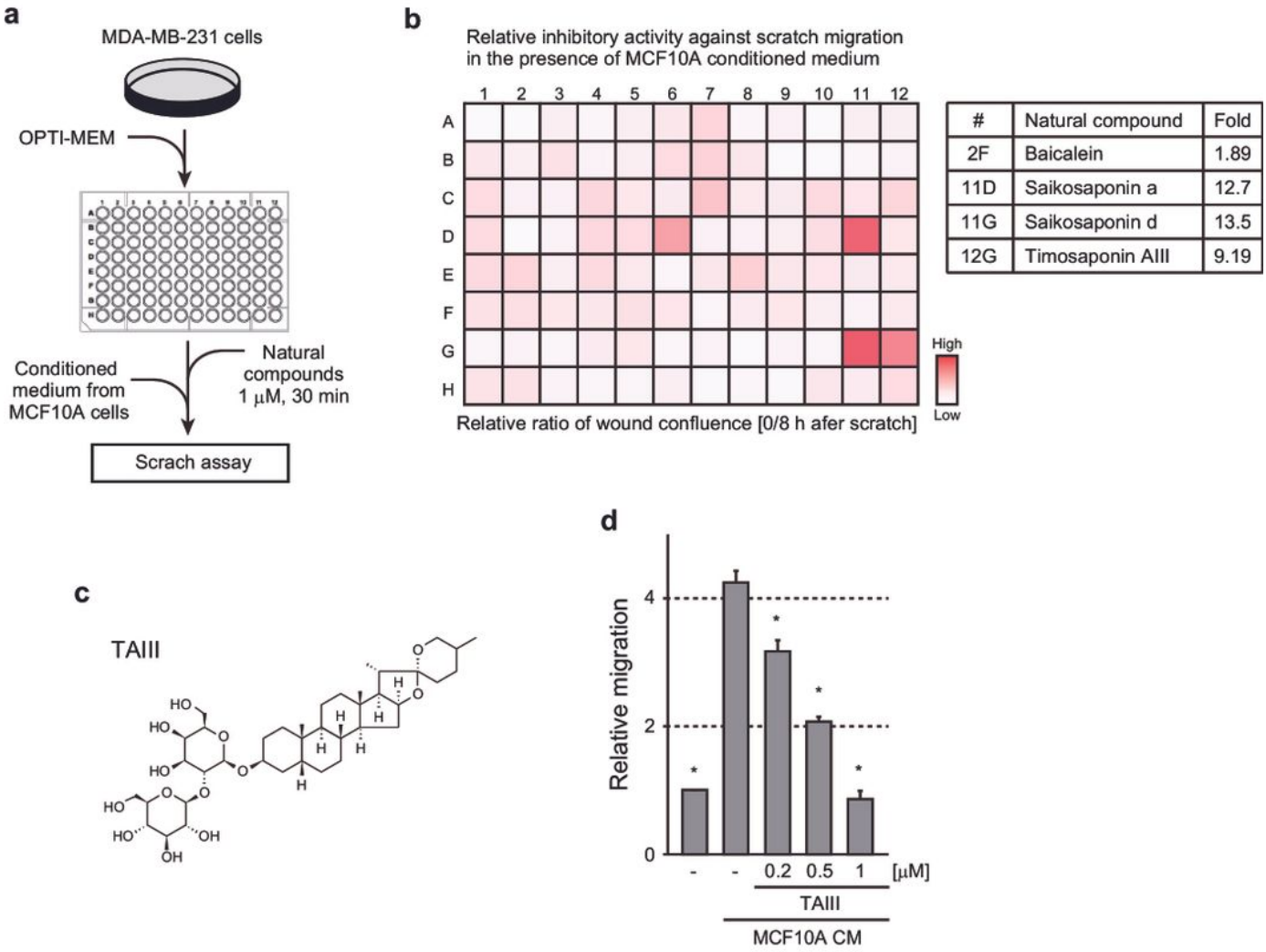

Figure 1 TAIII disturbed morphological changes and migration of breast adenocarcinoma cells induced by paracrine interactions with mammary epithelial cells.
a. Schematic experimental procedure for screening of natural compound library. MDA-MB-231 cells were plated in a 96-well culture plate under serum deprivation condition (OPTI-MEM). Cells were pretreated with each natural compound for 30 min and then treated with MCF10A CM and subjected to scratch assays. b. Heat map of the inhibitory activities of each compound. The relative inhibitory activity was calculated as the relative ratio of wound confluency at 0 h to 8 h and normalised by the value of DMSO. c. Structure of TAIII. d. MDA-MB-231 cells were subjected to Boyden chamber migration assays in the presence of MCF10A CM and indicated concentrations of TAIII. Each column shows the mean ± s.e.m. of three independent experiments. *p < 0.05 compared with cells treated with MCF10A CM alone.

Terabayashi et al.

Figure 1

TAIII disrupts morphological changes and migration of breast adenocarcinoma cells induced by paracrine interactions with mammary epithelial cells. a. Schematic experimental procedure for screening of natural compound library. MDA-MB-231 cells were plated in a 96-well culture plate under serum deprivation condition (OPTI-MEM). Cells were pretreated with each natural compound for 30 min and then treated with MCF10A CM and subjected to scratch assays. b. Heat map of the inhibitory activities of each

compound. The relative inhibitory activity was calculated as the relative ratio of wound confluency at 0 h to 8 h and normalised by the value of DMSO. c. Structure of TAIII. d. MDA-MB-231 cells were subjected to Boyden chamber migration assays in the presence of MCF10A CM and indicated concentrations of TAIII. Each column shows the mean ± s.e.m. of three independent experiments. *p < 0.05 compared with cells treated with MCF10A CM alone.

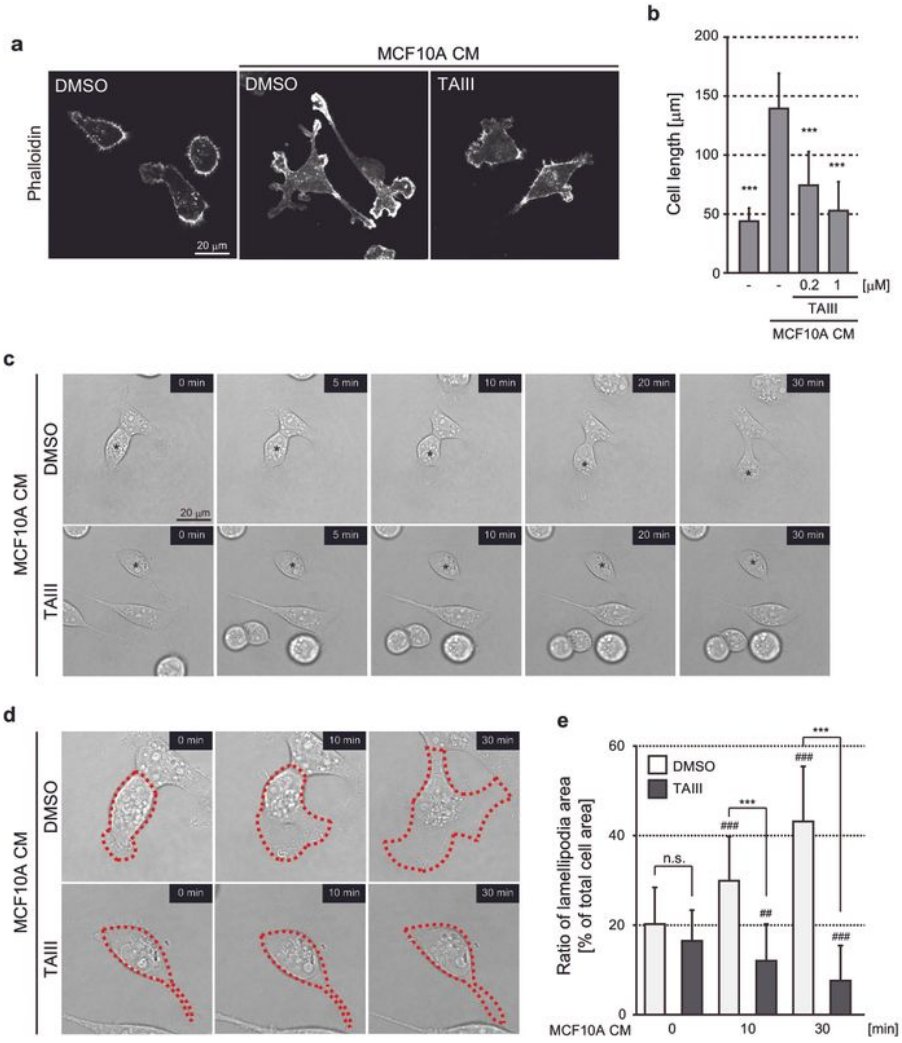

Figure 2 TAIII suppressed lamellipodia formation induced by MCF10A conditioned medium.
a. MDA-MB-231 cells treated with MCF10A CM in the presence of 1 μM TAIII for 1 h were fixed and stained with phalloidin. Scale bar: 20 μm. b. Quantification of the length of MDA-MB-231 cells treated with MCF10A CM in the presence of TAIII at the indicated concentrations for 1 h. Each column shows the mean ± s.e.m. of three independent experiments. ***p < 0.005 compared with cells treated with MCF10A CM alone. c. MDA-MB-231 cells were pretreated with DMSO or 1 μM TAIII and then further treated with MCF10A CM and observed under time-lapse phase-contrast microscopy. A series of images over the indicated time course is shown. Asterisks indicate identical cells among frames in each treatment. Scale bar: 20 μm. d. Magnified images of cells labelled with asterisks in (c) at the indicated time after MCF10A CM treatment. Total cell areas are outlined with dotted lines. e. The ratio of lamellipodia area after MCF10A CM treatment (n > 30). Each column shows the mean ± s.d. ##p < 0.01 and ###p < 0.005 compared with cells at 0 min in DMSO or TAIII treatment. ***p < 0.005 compared TAIII with DMSO treated cells at each time points.

Terabayashi et al.

Figure 2

TAIII suppresses lamellipodia formation induced by MCF10A CM. a. MDA-MB-231 cells were pretreated with DMSO or 1 μM TAIII and then further treated with MCF10A CM and observed under time-lapse phase-contrast microscopy. A series of images over the indicated time course is shown. Asterisks indicate identical cells among frames in each treatment. Scale bar: 20 μm. b. Magnified images of cells labelled with asterisks in (a) at the indicated time after MCF10A CM treatment. Total cell areas are outlined with dotted lines. c. The ratio of lamellipodia area after MCF10A CM treatment (n > 30). Each column shows the mean ± s.d. ##p < 0.01 and ###p < 0.005 compared with cells at 0 min in DMSO or TAIII treatment. ***p < 0.005 compared TAIII with DMSO treated cells at each time points.

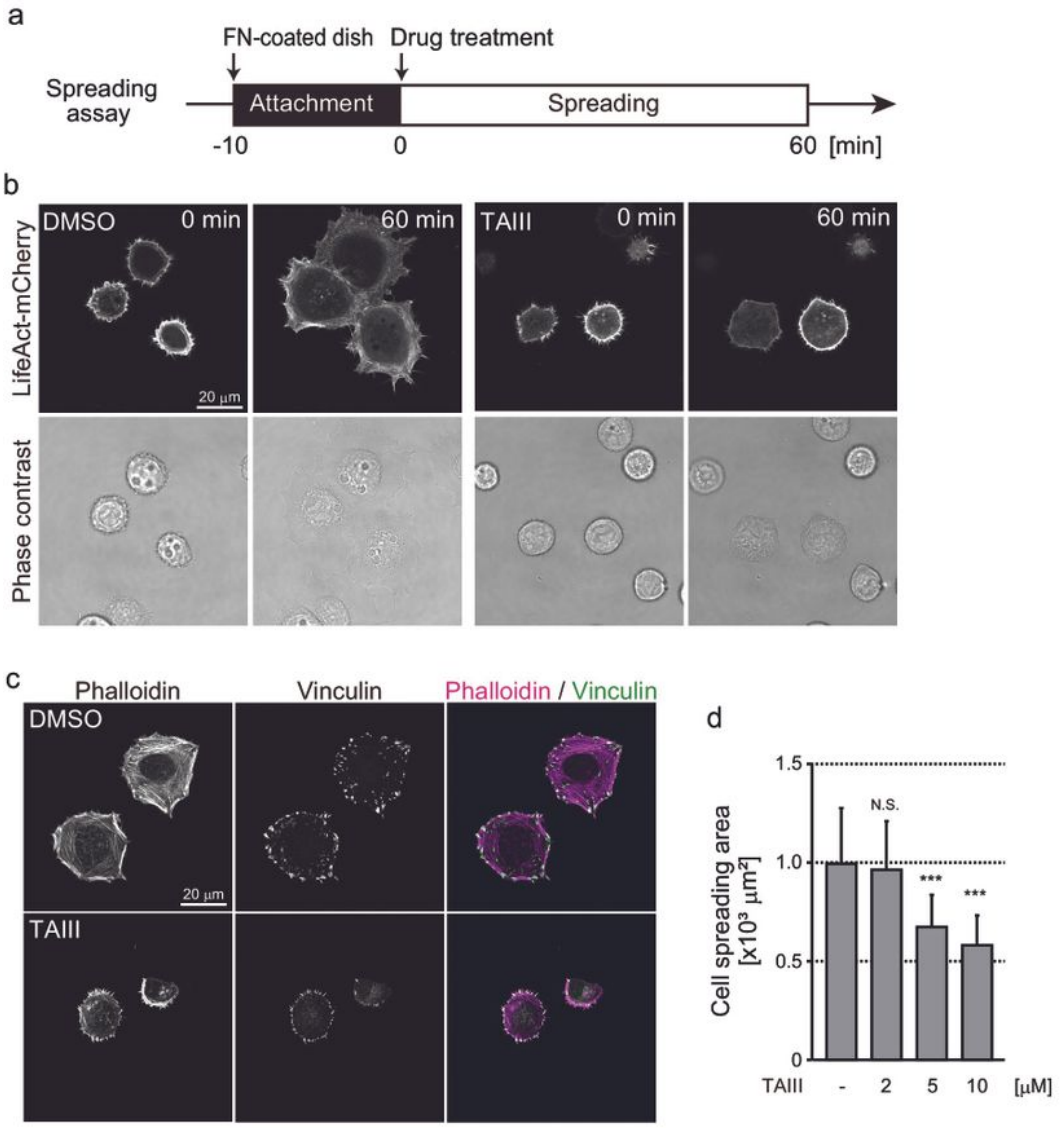

Figure 3 TAIII inhibited cell spreading on ECM.
a. Schematic experimental procedure for the cell-spreading assays in HeLa cells treated with TAIII. b. HeLa cells transfected with LifeAct-mCherry expression plasmid were plated onto fibronectin-coated dish. After attached, cells were treated with 10 μM TAIII and subjected to time-lapse imaging analysis. Fluorescence and phase contrast images were taken until 60 min after TAIII treatment. c. HeLa cells subjected to cell-spreading assay were fixed at 60 min after TAIII treatment and stained for vinculin and phalloidin. Bar; 20 μm. d. Quantification of cell spreading area at 60 min after TAIII treatment at the indicated concentrations. n > 30. Each column shows the mean ± s.d. ***p < 0.005 compared with cells treated with DMSO.

Terabayashi et al.

Figure 3

TAIII inhibits cell spreading on fibronectin. a. Schematic experimental procedure for the cell-spreading assays in HeLa cells treated with TAIII. b. HeLa cells transfected with LifeAct-mCherry expression plasmid were plated onto fibronectin-coated dish. After attached, cells were treated with 10 μM TAIII and subjected to time-lapse imaging analysis. Fluorescence and phase contrast images were taken until 60 min after TAIII treatment. c. HeLa cells subjected to cell-spreading assay were fixed at 60 min after TAIII treatment

and stained for vinculin and phalloidin. Bar; 20 μm. d. Quantification of cell spreading area at 60 min after TAIII treatment at the indicated concentrations. n > 30. Each column shows the mean ± s.d. ***p < 0.005 compared with cells treated with DMSO.

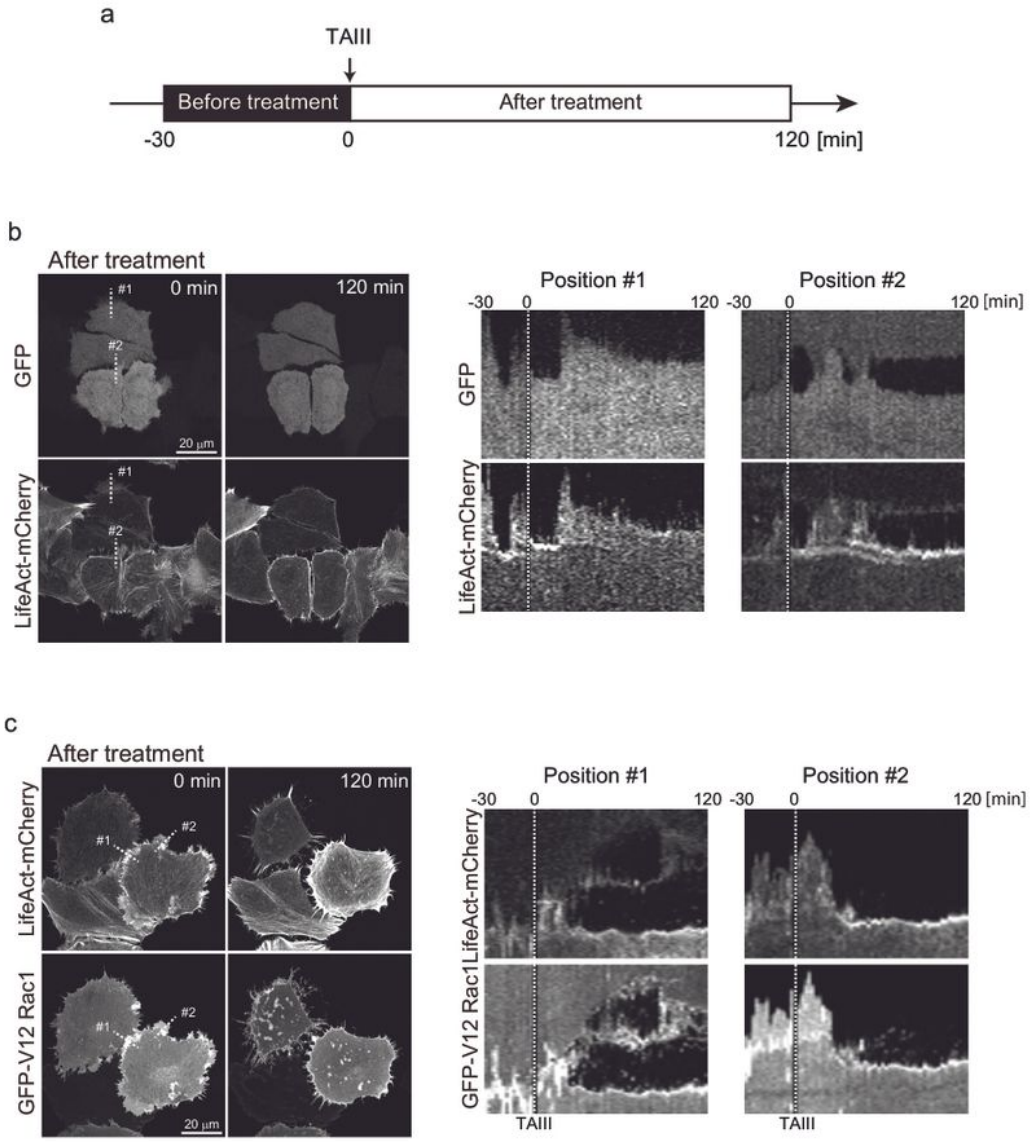

Figure 4 TAIII interfered with membrane dynamics regulated by Rac.
a. Schematic experimental procedure for time-lapse imaging analysis in HeLa cells treated with TAIII. b. HeLa cells transfected with GFP and LifeAct-mCherry expression plasmids. At 16 h post-transfection, the cells were subjected to time-lapse imaging analysis in the presence of TAIII treatment (10 μM). Left: representative images of transfected cells after TAIII treatment (0 and 120 min); scale bar: 20 μm. Right: kymograph analyses at dotted lines in the left panel. c. HeLa cells transfected with GFP-tagged constitutively active Rac1 (Val12) and LifeAct-mCherry expression plasmids were subjected to time-lapse imaging analysis as in (b). Left: representative images of transfected cells after TAIII treatment (0 and 120 min); scale bar: 20 μm. Right: kymograph analyses at dotted lines in the left panel.

Terabayashi et al.

Figure 4

TAIII interferes with membrane dynamics regulated by Rac. a. Schematic experimental procedure for time-lapse imaging analysis in HeLa cells treated with TAIII. b. HeLa cells transfected with GFP and LifeAct-

mCherry expression plasmids. At 16 h post-transfection, the cells were subjected to time-lapse imaging analysis in the presence of TAIII treatment (10 μM). Left: representative images of transfected cells after TAIII treatment (0 and 120 min); scale bar: 20 μm. Right: kymograph analyses at dotted lines in the left panel. c. HeLa cells transfected with GFP-tagged constitutively active Rac1 (Val12) and LifeAct-mCherry expression plasmids were subjected to time-lapse imaging analysis as in (b). Left: representative images of transfected cells after TAIII treatment (0 and 120 min); scale bar: 20 μm. Right: kymograph analyses at dotted lines in the left panel.

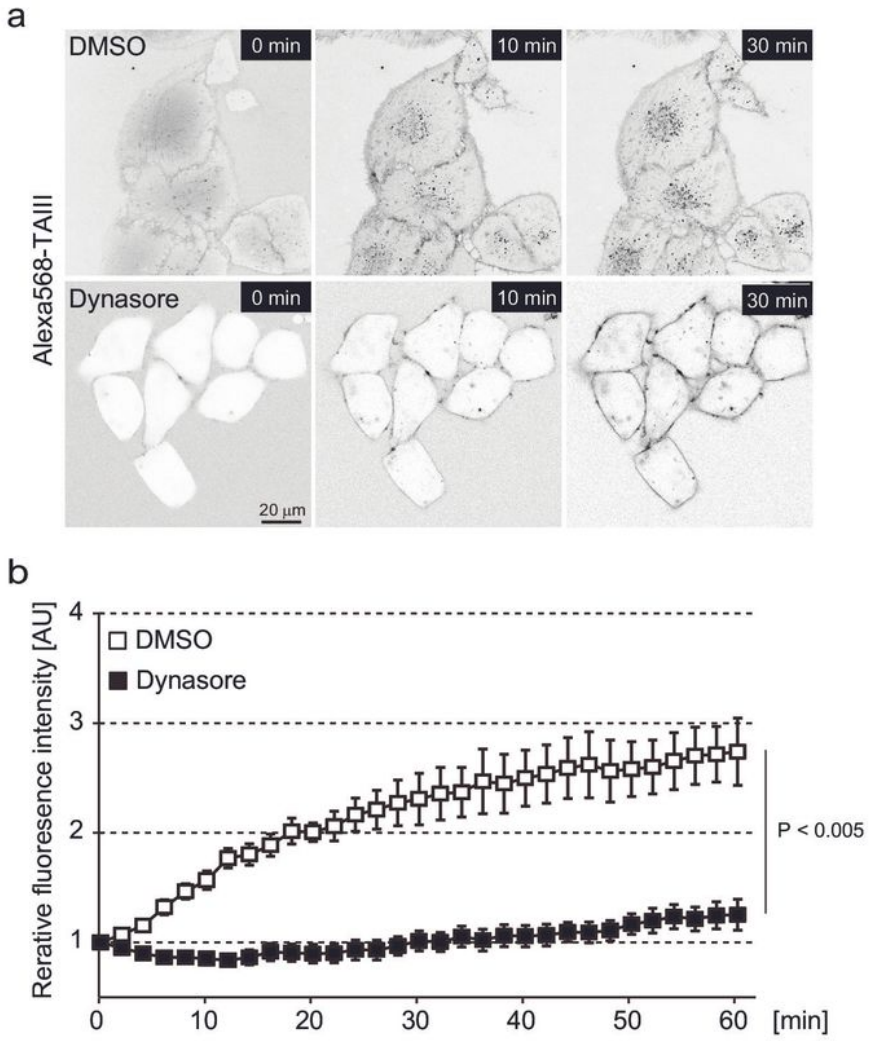

Figure 5 TAIII was internalised dependent on dynamin.
a. HeLa cells were treated with DMSO or dynasore (10 μM) for 6 h and further treated with Alexa Fluor 568 labelled-TAIII. Then, time-lapse imaging analysis was performed for 60 min. Representative images (0, 10 and 30 min after TAIII treatment) are presented. Scale bar: 20 μm. b. Quantification of signals intensity of internalised labelled-TAIII. Intensity of Alexa Fluor 568 normalized against levels at onset of 0 min. Data are presented as the mean ± s.e.m. (n>6). $p < 0.005$ at 60 min.

Terabayashi et al.

Figure 5

TAIII is internalised dependent on dynamin. a. HeLa cells were treated with DMSO or dynasore (100 μM) for 6 h and further treated with Alexa Fluor 568 labelled-TAIII. Then, time-lapse imaging analysis was performed for 60 min. Representative images (0, 10 and 30 min after TAIII treatment) are presented. Scale bar: 20 μm. b. Quantification of signals intensity of internalised labelled-TAIII. Intensity of Alexa Fluor 568 normalized against levels at onset of 0 min. Data are presented as the mean ± s.e.m. (n > 6). p < 0.005 at 60 min.

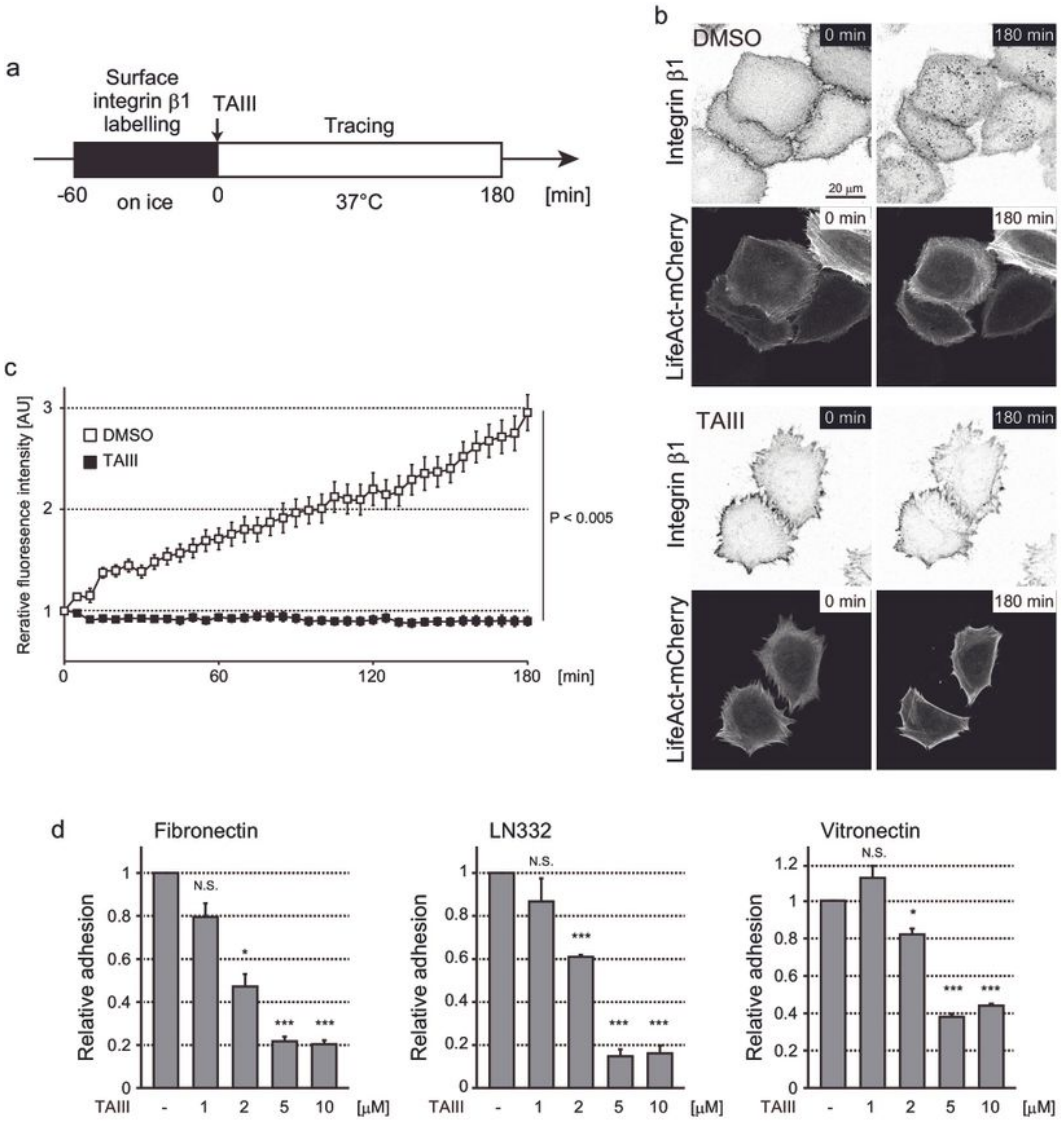

Figure 6 TAIII blocked integrin internalisation.
a. Schematic experimental procedure for the integrin internalisation assay. b. HeLa cells expressing LifeAct-mCherry plated onto fibronectin-coated dish were subjected to the integrin internalisation assay. Cells were analysed by time-lapse imaging analysis until 180 min after incubation at 37°C (tracing). Representative images of transfected cells after DMSO and TAIII treatment are shown. Scale bar: 20 μm. c. Quantifications of signal intensity of internalised integrin β1 after tracing. Intensity of Alexa Fluor 488 was normalized against levels at onset of tracing (0 min). Data are presented as the mean ± s.e.m. (n=20). p < 0.005 at 60 min. d. HeLa cells were trypsinised and treated with TAIII for 30 min at the indicated concentrations, and then subjected to adhesion assay. Each column shows the mean ± s.e.m. of three independent experiments. *p < 0.05, **p < 0.001 and ***p < 0.005 compared with cells treated with DMSO.

Terabayashi et al.

Figure 6

TAIII blocks integrin internalisation. a. Schematic experimental procedure for the integrin internalisation assay. b. HeLa cells expressing LifeAct-mCherry plated onto fibronectin-coated dish were subjected to the integrin internalisation assay. Cells were analysed by time-lapse imaging analysis until 180 min after incubation at 37°C (tracing). Representative images of transfected cells after DMSO and TAIII treatment are shown. Scale bar: 20 μm. c. Quantifications of signal intensity of internalised integrin β1 after tracing. Intensity of Alexa Fluor 488 was normalized against levels at onset of tracing (0 min). Data are presented as the mean ± s.e.m. (n=20). $p < 0.005$ at 60 min. d. HeLa cells were trypsinised and treated with TAIII for 30 min at the indicated concentrations, and then subjected to adhesion assay. Each column shows the mean ± s.e.m. of three independent experiments. *$p < 0.05$, **$p < 0.001$ and ***$p < 0.005$ compared with cells treated with DMSO.

Supplementary Files

This is a list of supplementary files associated with this preprint. Click to download.

- SupplementaryFigureS1.ai
- SupplementaryFigureS2.ai
- SupplementaryFigureS3.ai
- SupplementaryFigureS4.ai
- SupplementaryFigureS5.ai
- SupplementaryFigureS6.ai
- SupplementaryFigureS7.ai
- SupplementaryTableS1.ai
- SupplementaryVideo1.avi
- SupplementaryVideo10Rac1GFP.avi
- SupplementaryVideo11Rac1LifeAct.avi
- SupplementaryVideo12CDC42GFP.avi
- SupplementaryVideo13CDC42LifeAct.avi
- SupplementaryVideo14RhoAGFP.avi
- SupplementaryVideo15RhoALifeact.avi
- SupplementaryVideo16labelledTAIII.avi
- SupplementaryVideo17labelledTAIIIDynasore.avi
- SupplementaryVideo18DMSOintegrin.avi
- SupplementaryVideo19DMSOLifeAct.avi
- SupplementaryVideo2.avi

- SupplementaryVideo20TAIIIintegrin.avi
- SupplementaryVideo21TAIIILifeAct.avi
- SupplementaryVideo22Integrin.avi
- SupplementaryVideo23labelledTAIII.avi
- SupplementaryVideo24Integrin.avi
- SupplementaryVideo25labelledTAIII.avi
- SupplementaryVideo26Merge.avi
- SupplementaryVideo3.avi
- SupplementaryVideo4A431DMSO.avi
- SupplementaryVideo5A431TAIII.avi
- SupplementaryVideo6DMSO.avi
- SupplementaryVideo7TAIII.avi
- SupplementaryVideo8HeLaGFP.avi
- SupplementaryVideo9HeLaLifeAct.avi